Reconstruction of top quark pair dilepton decays in electron-positron collisions

Helenka Casler,[1,2] Matthew Manganel,[3] Miguel C. N. Fiolhais,[4,5] Andrea Ferroglia,[1,6] and António Onofre[7]

[1]*The Graduate School and University Center, The City University of New York, 365 Fifth Avenue, New York, New York 10016, USA*

[2]*Department of Earth and Physical Sciences, York College, City University of New York, 94—20 Guy R. Brewer Blvd., Jamaica, New York 11451, USA*

[3]*Courant Institute of Mathematical Sciences, New York University, 251 Mercer Street, New York, New York 10012, USA*

[4]*Science Department, Borough of Manhattan Community College, City University of New York, 199 Chambers Street, New York, New York 10007, USA*

[5]*LIP, Departamento de Física, Universidade de Coimbra, 3004-516 Coimbra, Portugal*

[6]*Physics Department, New York City College of Technology, The City University of New York, 300 Jay Street, Brooklyn, New York 11201, USA*

[7]*Departamento de Física, Universidade do Minho, 4710-057 Braga, Portugal*

(Received 6 February 2019; published 18 March 2019)

A new algorithm is presented to perform the full kinematic reconstruction of top quark pair events produced at future electron-positron colliders in the case of dilepton decays of the W bosons to electrons or muons. The momentum components of the undetected neutrino and antineutrino in the event are reconstructed by employing several kinematic conditions comprising a nonlinear system of six equations. This system is solved numerically using two independent methods, and the selection of the best candidate real solution for each event is determined by a likelihood discriminant. Results are presented for several reconstructed kinematic properties of the $W^{\pm}$ bosons, top (and antitop) quarks using generator level information produced at leading order.

DOI: 10.1103/PhysRevD.99.054011

I. INTRODUCTION

While the LHC is producing extremely precise measurements of top quark and Higgs boson properties, the planning for the next high energy particle accelerator is already underway. The objective of the planning and designing work is to develop a machine able to investigate in depth beyond the Standard Model (SM) physics scenarios. Despite the fact that there is no decision yet to determine which accelerator will be built, or its location, there is a consensus in the scientific community that the results from the LHC will have to be complemented by an accelerator that can measure observables with greater precision by producing high energy collisions between electrons and positrons. At present, the most likely candidates are the International Linear Collider (ILC) [1], the Compact Linear Collider (CLIC) [2], and the Future Circular Collider (FCC) [3,4]. The ILC is expected to operate at a center-of-mass energy of 500 GeV with a possible upgrade to 1 TeV. CLIC is designed to collide electrons and positrons at a nominal energy of 3 TeV, while FCC is expected to operate with a center-of-mass energy in the range of 90–350 GeV.

Future electron-positron accelerators comprise several advantages which allow for high-precision phenomenological studies in Higgs boson processes, studies of top-quark pair production, and searches for new particles. One of the advantages provided by an electron-positron machine is the ability to operate within a wide range of center-of-mass energies. An electron-positron collider also makes it possible to collide electron and positron beams with high spin polarization. This feature opens the window to several new observables that could not be measured using hadron colliders [5,6]. In addition, high energy collisions in electron-positron accelerators are less complex when compared to proton-proton collisions. As a result, particle detectors in electron-positron colliders have higher intrinsic resolution than those at machines colliding protons.

The reconstruction of neutrinos is one of the main experimental challenges in high energy physics experiments as they do not interact with the active material of the particle detector. As such, the momenta of the neutrinos are normally associated with the missing momentum in the

event resulting from a high-energy collision. This leads to a straightforward reconstruction if only a single neutrino (or antineutrino) is produced in the physics process of interest. The reconstruction becomes highly nontrivial if two or more neutrinos are produced. This particular problem has been successfully addressed at the LHC in top-quark pair production and Higgs boson production in association with a top-quark pair. The full kinematic reconstruction of the four-momenta of the undetected neutrinos was performed by imposing energy-momentum conservation and using mass constraints on the top quarks and $W^{\pm}$ bosons [7–10].

In this paper, a similar strategy is implemented in order to develop an algorithm to reconstruct the momentum of the neutrino (and antineutrino) resulting from the dilepton decay of a top-quark pair ($t\bar{t}$) produced in an electron-positron collision. By using the momenta of all detected final state particles resulting from the top and antitop quark decays, a system of six kinematic equations is implemented in order to determine the unknown momenta of the neutrino and antineutrino. The system is solved by using two different numerical methods applied to 1×10^6 event samples generated with `MadGraph5_aMC@NLO` at leading order [11]. This particular nonlinear system of equations leads to multiple possible complex and real solutions for the neutrino's momenta. Consequently, an extensive statistical study is performed to determine which physical variables are the best decision-making indicators to choose the best candidate real solution by means of a likelihood method. Results are presented by comparing several reconstructed kinematic properties such as the transverse momentum and masses of the (anti)top quarks and $W^{\pm}$ bosons with the generator level information provided by `MadGraph5_aMC@NLO`. This study is performed at parton level for events which have tree-level kinematics. The effects of background events, beam resolution, radiation, detector simulation, and selection cuts are beyond the scope of the manuscript, and are therefore deferred to a future study. The reconstruction code packages are made available in public repositories [12,13].

II. KINEMATIC EQUATIONS

The reconstruction of $t\bar{t}$ dilepton events assumes the experimental detection of two b-tagged jets and two opposite charged leptons together with the measurement of missing energy associated with the neutrino and antineutrino. Neutrinos are not detected as they escape without interacting with the active material of the detector. Consequently, the neutrino momenta can be associated with the missing energy. Using the mass of the $W^{\pm}$ bosons as constraints, and assuming the approximation that all final state particles are massless, the three-momenta of the neutrino and antineutrino can be determined from six kinematic equations. To begin with, three linear equations can be written as

$$p_i^{\nu} + p_i^{\bar{\nu}} = p_i^{\text{miss}}, \tag{1}$$

where p_i^{miss} represents the components of the missing momentum, and p_i^{ν} and $p_i^{\bar{\nu}}$ correspond to the neutrino and antineutrino momentum components, respectively. Conservation of center-of-mass energy at the collision point, $\sqrt{s}$, is employed to obtain a nonlinear equation:

$$E^{\ell^-} + E^{\ell^+} + E^{\nu} + E^{\bar{\nu}} + E^{b} + E^{\bar{b}} = \sqrt{s}, \tag{2}$$

where E^i represents the energy of the particle i. It should be stressed that the nominal center-of-mass energy of the collider might differ from the effective center-of-mass energy of the electron-positron collision due to beamstrahlung and initial state radiation (ISR). A recent study has shown that CLIC is expected to deliver 38% of the total luminosity above 99% of the nominal center-of-mass energy at 1.5 TeV and 60% of the total luminosity at 380 GeV [14]. This may lead to a degradation of the reconstruction efficiency in events with an emission of photons that escape the main detector, i.e., collinear with the incoming beams. Nonetheless, recent studies on the prospective measurement of the top quark mass at future electron-positron collider detectors show a successful reconstruction of $t\bar{t}$ events when imposing the nominal center-of-mass energy as a constraint [15–17]. These studies were performed in both hadronic and leptonic final states using full detector simulation and taking into account the effects of beamstrahlung and ISR. In addition, future electron-positron collider experiments are also expected to deliver the precise measurement of the effective center-of-mass energy of the electron-positron collision after beamstrahlung and ISR, which would open the possibility to implement the reconstruction procedure in $t\bar{t}$ radiative events with a collision energy below the nominal center-of-mass energy [14]. In this case, the event-by-event effective collision center-of-mass energy should be used in Eq. (2), instead of the nominal center-of-mass energy. A similar strategy was employed at LEP II, where the collision center-of-mass energy was used to set the scale for the W boson mass measurement in W pair production events. The effective center-of-mass energy after beamstrahlung and ISR was precisely reconstructed on an event-by-event basis for both leptonic and hadronic final state topologies [18].

Finally, the $W^{\pm}$ boson masses are constrained to a fixed value, $m_W = 80.4$ GeV, leading to two additional quadratic kinematic equations,

$$\begin{aligned} (p^{\ell^-} + p^{\bar{\nu}})^2 &= m_W^2, \\ (p^{\ell^+} + p^{\nu})^2 &= m_W^2, \end{aligned} \tag{3}$$

where $p = (E, \vec{p})$ represents the four-vector of the particles. The input value of the W boson invariant mass in Eq. (3), m_W, can be changed in the code from its default

value in order to increase the number of events with at least one real solution. The input value can be fluctuated within a certain mass range until the reconstruction procedure finds a real solution for a given event. The window in which the invariant mass should be fluctuated must be chosen according to the expected resolution for the W boson mass distribution in the electron-positron collider detector under study. A similar approach has been implemented at the LHC for the reconstruction of $t\bar{t}$ dilepton events, in which the input value of the top quark mass is fluctuated in order to increase the number of events with real solutions [7].

These six kinematic equations can be used to determine a total of six unknown momentum components for the neutrino and antineutrino. However, due to the presence of two quadratic equations (3) and one polynomial equation (2) with nested radicals, it is hard to retrieve a set of analytic solutions from this kinematic system of equations. Nonetheless, the analytic elimination of five out of the six unknown variables leads to two implicit nonlinear equations for the same unknown quantity, which is taken to be p_z^ν. The physical value of p_z^ν is a solution of one of these two equations.

The six kinematic equations are significantly different from the ones used at the LHC for the top quark pair production in the same decay channel [7–10]. In particular, at the LHC the total linear momentum of the final state particles caught by the detector and the neutrinos is only zero on the transverse plane, and not along the collision line (z axis). Furthermore, since the proton is not an elementary particle, the center-of-mass energy of the $t\bar{t}$ system is unknown. As a result, the kinematic equations for the reconstruction at the LHC require (anti)top quark mass constraints, while the reconstruction at the electron-positron collider can be performed without imposing any condition on the kinematics of the (anti)top quarks.

Even though this reconstruction procedure is not recommended for events with additional objects, such as additional jets, it can be applied to more inclusive signal regions, provided that the energy of these additional jets is subtracted from the collision center-of-mass energy in Eq. (2). However, despite the fact that a more inclusive selection allowing for three or more jets would increase the amount of selected events, it would at the same time degrade the reconstruction and related systematic uncertainties. Nonetheless, similar parton level reconstruction methods have been implemented in inclusive analyses with more than two jets in $t\bar{t}$ dilepton final states at the LHC [7]. The efficiency of the parton level reconstruction algorithm presented in this paper can be tested in the future with events including next-to-leading order (NLO) corrections for the fully decayed final state [19].

III. EVENT RECONSTRUCTION

While it is difficult to retrieve an analytic solution from the system of equations presented in the previous section, it is possible to obtain numerical solutions on an event-by-event basis. As such, two numerical methods were implemented and compared to make sure they provide consistent results. Both methods were applied to a sample of 1×10^6 $e^-e^+ \to t\bar{t} \to W^+W^-b\bar{b} \to \ell^+\ell^-\nu\bar{\nu}b\bar{b}$ events generated with `MadGraph5_aMC@NLO` at leading order at a center-of-mass energy of 1 TeV. This sample was labeled as Sample A. The events in this sample were generated with massless final state particles, with the exception of the bottom quarks. The mass of the bottom quarks was set to its on-shell value of 4.7 GeV. In the rest of this work, the adjective "generated" refers to the list of events and momenta obtained from `MadGraph5_aMC@NLO` as explained above.

The two implicit equations for p_z^ν were treated as distinct problems to be solved individually. For each event, the equations were put in the form

$$f_i(p_z^\nu) = 0, \qquad i = 1, 2. \tag{4}$$

In the first approach, a bisection method was used to find the real solutions of Eq. (4). The allowed range of p_z^ν was limited to the real domain of the $f_i(p_z^\nu)$. This range was bisected in search of solutions until the remaining range was less than 1% the size of the original range. Each one of the functions in Eq. (4) was found to have one real solution at most.

For the second approach, the functions $f_i(p_z^\nu)$ were approximated by interpolating each function with a degree-four polynomial within the allowed range of values for p_z^ν. While analytic solutions to these polynomials exist, it is more efficient to solve them numerically using the method documented in [20]. Once the functions are interpolated, the roots of the polynomials should coincide with those of the original functions, provided the interpolation error is small. Therefore, to confirm that the polynomials adequately approximate the functions, the adjusted R-squared coefficient is calculated using a set of 50 test points for each interpolation. Solutions were only taken from interpolants with an R-squared coefficient of 0.95 or greater. In 1×10^6 events, all but a single R-squared coefficient fell above this threshold. A degree of 4 was chosen because it is the smallest polynomial degree that fits $f_i(p_z^\nu)$ with this level of precision.

The results of both methods are statistically compatible, with no real solution found for 12% of all events, one real solution found with a frequency of 23%, and two real solutions per event found for the remaining 65% of events. As a first step, in the case of an event with two possible real solutions, the solution to be considered in the reconstruction was selected randomly. (In Sec. IV, a likelihood method is introduced to select the most likely solution.) Figure 1 shows the correlation plots between the generated (anti)neutrino transverse and z-axis momentum components and their reconstructed values. The correlation between the generated

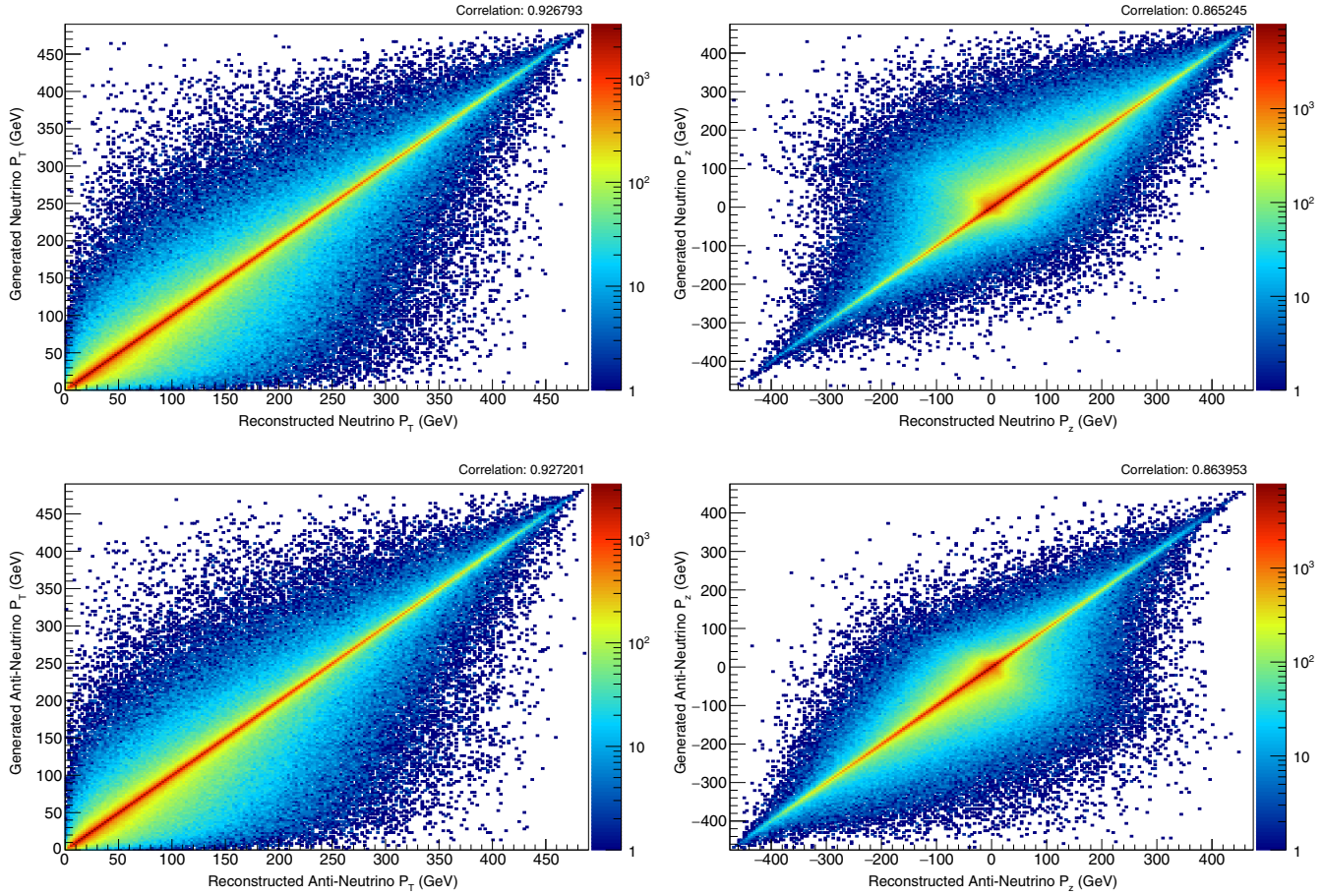

FIG. 1. Correlation plots between the generated and reconstructed transverse (left) and z-axis (right) momentum components of the neutrino (top) and antineutrino (bottom). These plots were produced with Sample A.

and reconstructed neutrino kinematic variables is above 85%, which indicates a successful reconstruction. It is also worth noting that the asymmetry seen between the z-axis momentum components of the neutrino and antineutrino is merely a consequence of the direction of the electron and positron beams upon the collision. In fact, because of the forward-backward asymmetry induced by the weak interaction, top quarks (and consequently neutrinos) are preferably emitted in the direction of the incoming electron, while antitop quarks are preferably emitted in the direction of the

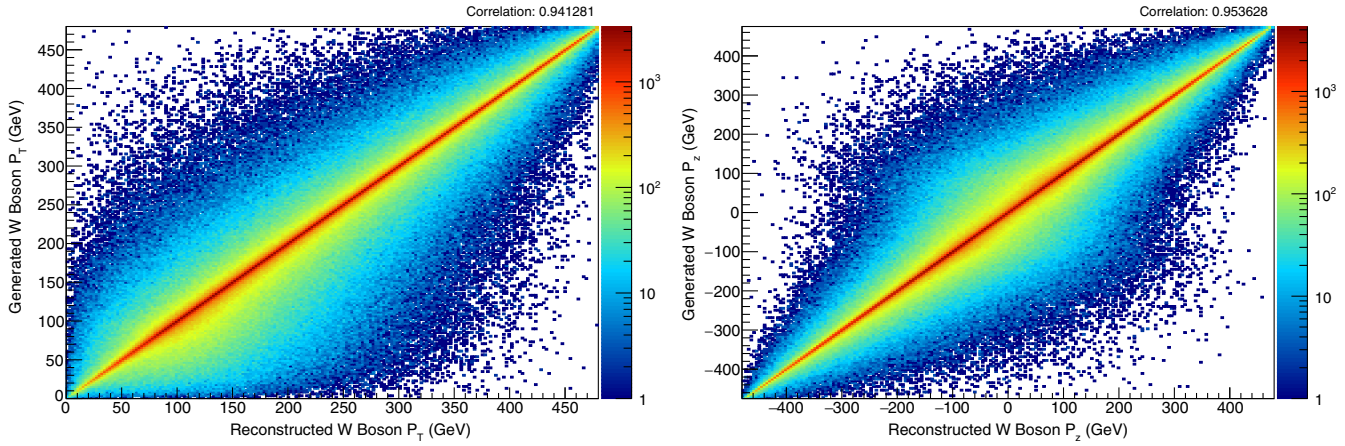

FIG. 2. Correlation plots between the generated and reconstructed transverse (left) and z-axis (right) momentum components of the $W^{\pm}$ bosons. These plots were produced with Sample A.

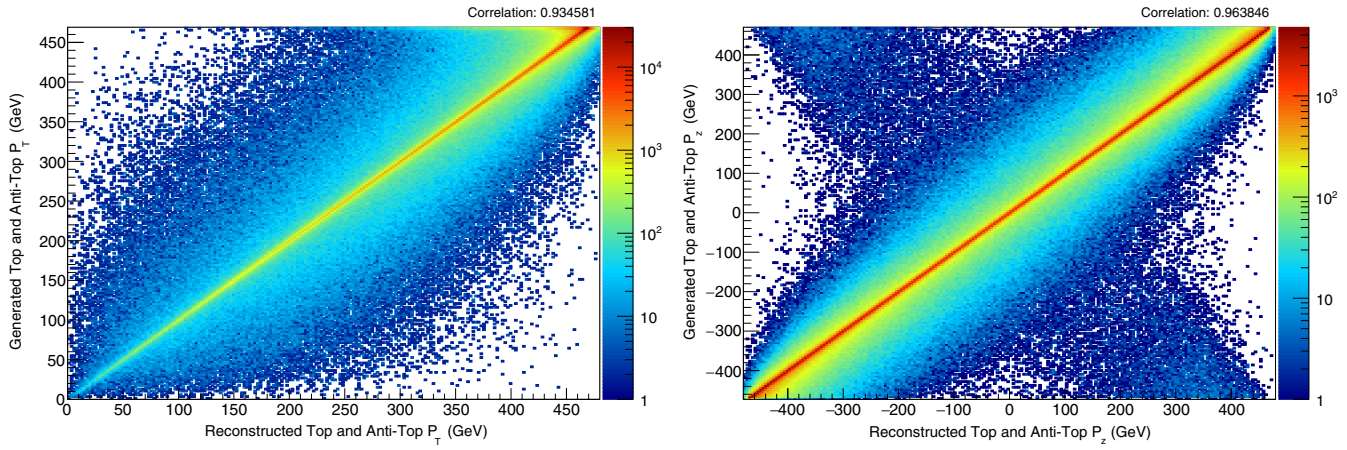

FIG. 3. Correlation plots between the generated and reconstructed transverse (left) and z-axis (right) momentum components of the top and antitop quarks. These plots were produced with Sample A.

incoming positron. As expected, the correlations between the generated and reconstructed transverse and z-axis momentum components of the $W^{\pm}$ bosons, shown in Fig. 2, are similar to the ones of the neutrinos.

The ultimate goal of this procedure is to fully reconstruct the momentum of the top and antitop quarks. Since the charge of the $b(\bar{b})$ jet is assumed to be unknown in the experimental analysis, one faces the problem of pairing the $b(\bar{b})$ quark with the charged lepton resulting from the same $t(\bar{t})$ decay. For each solution there are only two different pairing possibilities and the most likely pair is determined by means of a χ^2 method. The χ^2 variable employed in the code is defined as

$$\chi^2 = \frac{(m_t^{\mathrm{rec}} - m_t)^2}{\Gamma_t^2} + \frac{(m_{\bar{t}}^{\mathrm{rec}} - m_{\bar{t}})^2}{\Gamma_{\bar{t}}^2}, \tag{5}$$

where m_t^{rec} and $m_{\bar{t}}^{\mathrm{rec}}$ are the reconstructed top and antitop quark mass, respectively, with $m_t = m_{\bar{t}} = 173.2$ GeV and $\Gamma_t = \Gamma_{\bar{t}} = 1.42$ GeV [21]. The most likely pair candidate is determined by the lowest χ^2 value. The correlation plots between the generated and reconstructed transverse and z-axis momentum components of the top and antitop quarks are presented in Fig. 3. The z-axis momentum of the (anti)top quarks on the right-hand side plot shows a residual anticorrelation. The source of this anticorrelation was traced back to cases of wrong pairing between the $b(\bar{b})$ quarks and the charged leptons. This problem can be addressed in the future by implementing more sophisticated statistical methods to establish the b-jet pairing.

IV. LIKELIHOOD METHOD

Since the system of kinematic equations may lead to two possible real solutions roughly 65% of the time, one of the main challenges of the reconstruction procedure is to pick the right solution in these cases. In this study, a likelihood discriminant method was implemented in order to determine the most likely solution. For each solution a likelihood variable, $\mathcal{L}$, is calculated as the product of several probability density functions (p.d.f., indicated with P below). Three p.d.f.s were built from the top and antitop quark kinematic variables, mass (m_t), transverse momentum ($p_{\mathrm{T},t}$), and z-axis momentum component ($p_{\mathrm{z},t}$),

$$\mathcal{L} = P(m_t)P(p_{\mathrm{T},t})P(p_{\mathrm{z},t}). \tag{6}$$

The p.d.f.s in Eq. (6) were obtained by using an additional sample of 1×10^6 events generated with `MadGraph5_aMC@NLO` at leading order, labeled as Sample B. Events in Sample B were generated assuming massless final state particles, with the exception of the bottom quarks, exactly as it was done for Sample A. Each solution for a given event in Sample B was assigned a "good" or "bad" label, based on the proximity between the reconstructed and generated (anti)neutrino. The proximity criteria between the reconstructed and generated (anti)neutrino is determined by means of a χ^2 variable,

$$\chi^2 = \sum_{i=1}^{3} \frac{(p_i^{\nu,\mathrm{rec}} - p_i^{\nu,\mathrm{gen}})^2}{s} + \frac{(p_i^{\bar{\nu},\mathrm{rec}} - p_i^{\bar{\nu},\mathrm{gen}})^2}{s}, \tag{7}$$

where $p_i^{\nu,\mathrm{rec}}$ and $p_i^{\bar{\nu},\mathrm{rec}}$ correspond to the reconstructed neutrino and antineutrino momentum components, respectively. The generated neutrino and antineutrino momentum components are represented by $p_i^{\nu,\mathrm{gen}}$ and $p_i^{\bar{\nu},\mathrm{gen}}$, respectively.

The (anti)top quark mass p.d.f. distribution is shown in Fig. 4, where the blue shaded histogram represents the distribution for the good solutions and the red shaded histogram represents the distribution for the bad solutions. The difference in shape of the p.d.f.s for good and bad solutions provides significant discriminating power. The p.d.f.s were then used to calculate the likelihood variables for each solution of every event with two possible real

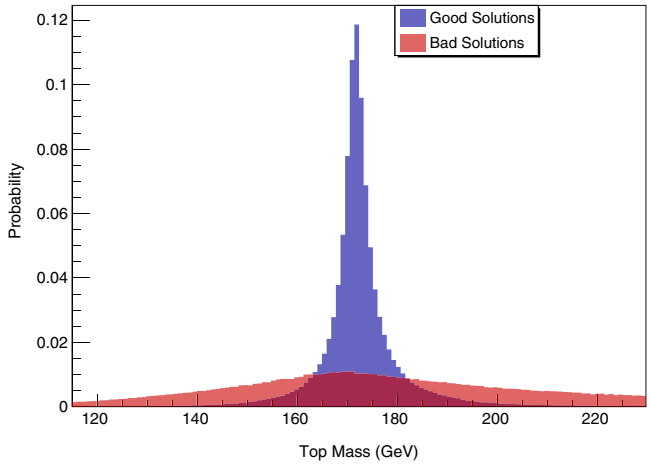

FIG. 4. Probability density functions (p.d.f.) of the (anti)top quark mass. The blue shade represents the distribution for the "good" solutions, and the red shade represents the distribution for the "bad" solutions. These plots were produced with Sample B.

solutions in Sample A. For each event solution in Sample A, the likelihood of that solution being good, $\mathcal{L}_G$, can be calculated as the product of the good solution p.d.f.s, using Eq. (6). In a similar fashion, the likelihood of that solution being bad, $\mathcal{L}_B$, can also be calculated as the product of the bad solution p.d.f.s. Therefore, each event solution has a likelihood of being good and bad. For each event, the solution with higher likelihood ratio, $\mathcal{L}_G/\mathcal{L}_B$, is picked as the most likely candidate to be the good solution.

Results obtained with Sample A are presented in Figs. 5–7. Figure 5 shows the correlation plots between the generated (anti)neutrino transverse and z-axis momentum components and their reconstructed values after applying the likelihood discriminant method. A correlation of about 95% is obtained for these kinematic variables, a significant improvement when compared with the results of Fig. 1. A clear improvement is also seen in the reconstruction of the $W^{\pm}$ bosons, shown in Fig. 6. Figure 7 shows the comparison between the generated (anti)top transverse and z-axis momentum components and their reconstructed values. A correlation above 95% clearly indicates a successful reconstruction of the kinematic properties of this particle. The correlation between these reconstructed and generated kinematic variables can be further increased by applying a selection cut on the likelihood ratio variable. Similar results can be achieved with other discriminant

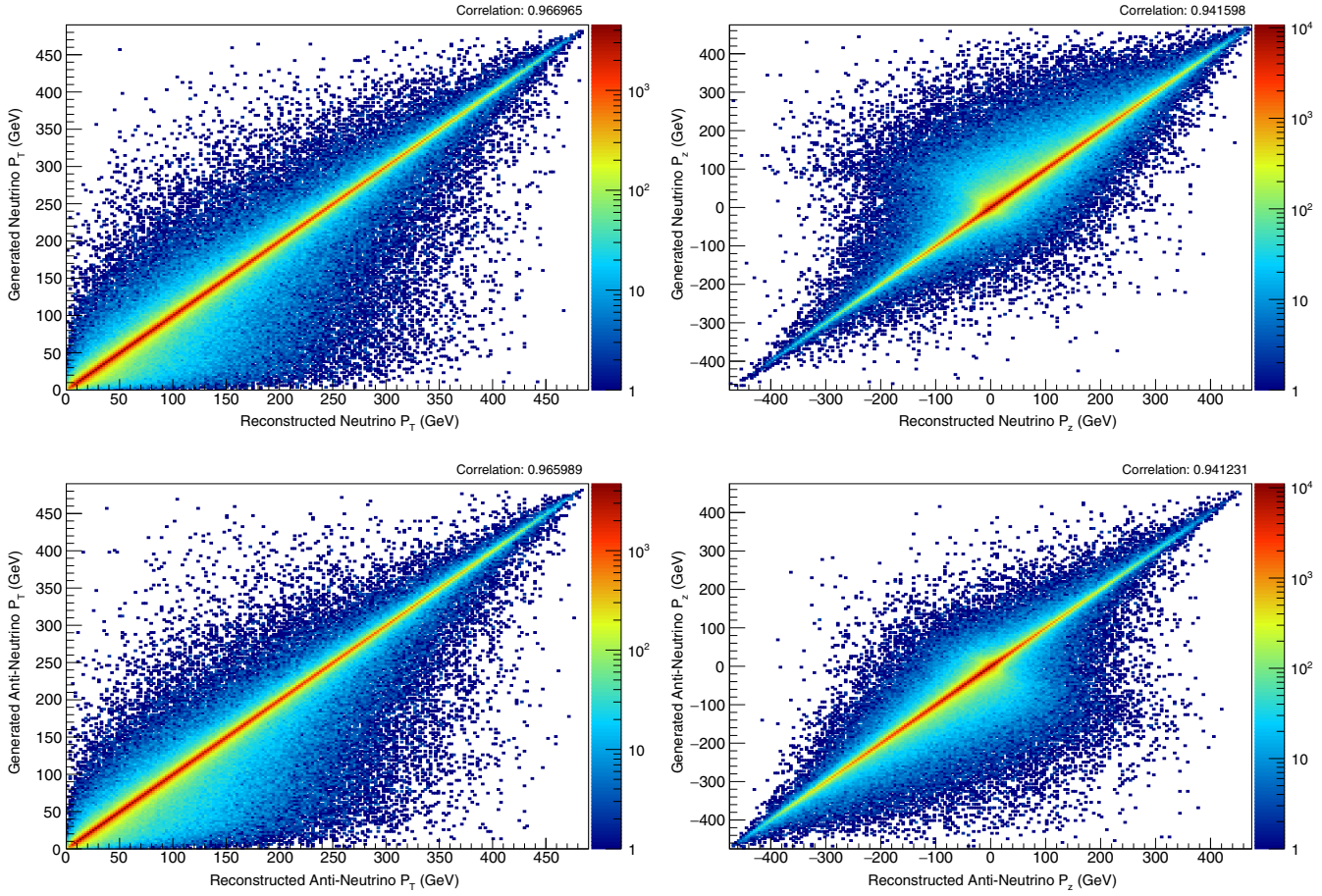

FIG. 5. Correlation plots between the generated and reconstructed transverse (left) and z-axis (right) momentum components of the neutrino (top) and antineutrino (bottom) after applying the likelihood method. These plots were produced with Sample A.

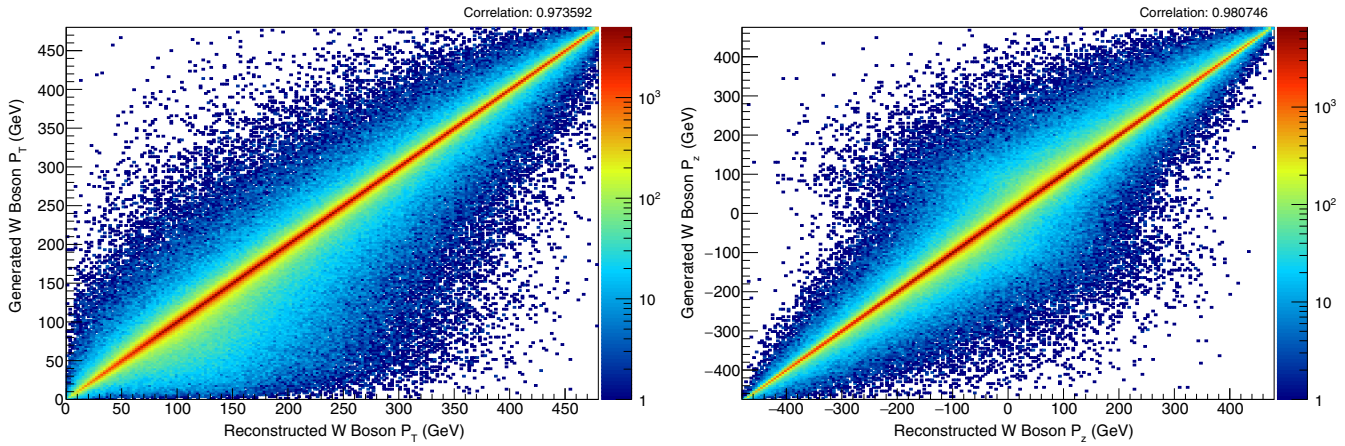

FIG. 6. Correlation plots between the generated and reconstructed transverse (left) and z-axis (right) momentum components of the $W^{\pm}$ bosons after applying the likelihood method. These plots were produced with Sample A.

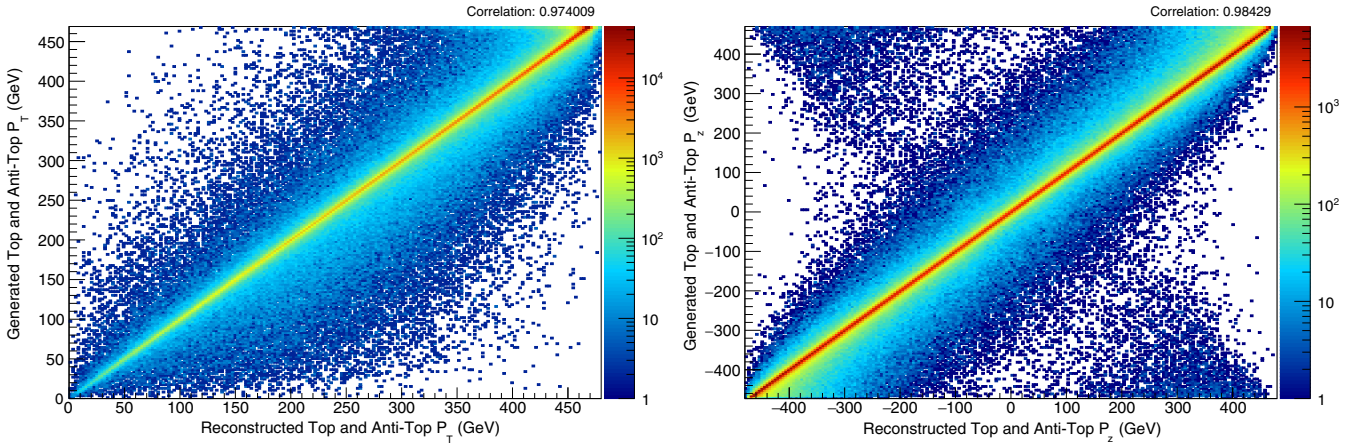

FIG. 7. Correlation plots between the generated and reconstructed transverse (left) and z-axis (right) momentum components of the top and antitop quarks after applying the likelihood method. These plots were produced with Sample A.

methods such as neural networks or multivariate analyses [22]. It should be stressed, however, that the effect of beam resolution, detector acceptance, and selection cuts are expected to have an impact on the efficiency of the reconstruction procedure.

V. CONCLUSIONS

The goal of the present paper was to implement a method which allows for the reconstruction of the (anti)neutrino momentum components in the dileptonic decays of a top-quark pair at future electron-positron colliders.

Two independent numerical methods were implemented for this purpose. The reconstruction code packages were thoroughly tested using generated samples of 1×10^6 electron-positron collision events at a center-of-mass energy of 1 TeV. The packages are publicly available, and they can be downloaded from a repository [12,13].

In addition, a likelihood method was implemented to determine the most likely solution in each event. If the likelihood method is applied, the correlation for the reconstructed (anti)neutrino, the (anti)top quarks, and $W^{\pm}$ bosons is above 95%. The effectiveness of the reconstruction package with and without the likelihood method can be evinced from the correlation plots found in Secs. III and IV.

The next step of this study will be to implement this reconstruction method in a dedicated analysis, in order to perform measurement estimations of top quark properties at future electron-positron colliders. These estimations may include the study of top quark spin correlations, $W^{\pm}$ boson polarization in top quark decays, and the top quark forward-backward asymmetry. This will require the simulation of a general purpose detector, the implementation of an event selection, and a detailed study of the different sources of systematic uncertainties.

ACKNOWLEDGMENTS

The authors thank the Center for Theoretical Physics of the Physics Department at the New York City College of Technology, for providing computing power from their

High-Performance Computing Cluster. This work was funded by PSC-CUNY Awards No. 61085-00 49 and No. 61151-00 49, and by FCT, Lisboa 2020, Compete 2020, Portugal 2020, FEDER through Project No. POCI/01-0145-FEDER-029147. The work of A. F. was supported in part by the National Science Foundation under Grant No. PHY-1417354. The work of H. C. was supported in part by the Department of Energy under Grant No. DE-SC0019027. The authors thank N. Castro for useful discussions and for reading the manuscript.

[1] T. Behnke *et al.*, arXiv:1306.6327.
[2] L. Linssen, A. Miyamoto, M. Stanitzki, and H. Weerts, arXiv:1202.5940.
[3] M. Benedikt *et al.*, Future Circular Collider (FCC) Report No. CERN-ACC-2019-0003, 2019.
[4] J. Ellis and T. You, J. High Energy Phys. 03 (2016) 089.
[5] J. A. Aguilar-Saavedra, M. C. N. Fiolhais, and A. Onofre, J. High Energy Phys. 07 (2012) 180.
[6] M. C. N. Fiolhais, J. Phys. Conf. Ser. **447** 034021 (2013).
[7] G. Aad *et al.* (ATLAS Collaboration), J. High Energy Phys. 06 (2012) 088.
[8] S. P. Amor dos Santos *et al.*, Phys. Rev. D **92**, 034021 (2015).
[9] S. Amor Dos Santos *et al.*, Phys. Rev. D **96**, 013004 (2017).
[10] D. Azevedo, A. Onofre, F. Filthaut, and R. Gonçalo, Phys. Rev. D **98**, 033004 (2018).
[11] J. Alwall, R. Frederix, S. Frixione, V. Hirschi, F. Maltoni, O. Mattelaer, H.-S. Shao, T. Stelzer, P. Torrielli, and M. Zaro, J. High Energy Phys. 07 (2014) 079.
[12] https://github.com/HCasler/NeutrinoBisect.
[13] https://github.com/mmanganel/neurecon.
[14] H. Abramowicz *et al.* (CLICdp Collaboration), arXiv:1807.02441.
[15] K. Seidel, S. Poss, and F. Simon, European Organization for Nuclear Research (CERN) Report No. LCD-2011-026, 2012.
[16] K. Seidel, F. Simon, M. Tesar, and S. Poss, Eur. Phys. J. C **73**, 2530 (2013).
[17] M. Beckmann, B. List, and J. List, Nucl. Instrum. Methods Phys. Res., Sect. A **624**, 184 (2010).
[18] J. Abdallah *et al.* (DELPHI Collaboration), Eur. Phys. J. C **34**, 127 (2004).
[19] B. Chokoufé Nejad, W. Kilian, J. M. Lindert, S. Pozzorini, J. Reuter, and C. Weiss, J. High Energy Phys. 12 (2016) 075.
[20] https://docs.scipy.org/doc/numpy-1.15.0/reference/generated/numpy.roots.html.
[21] V. Khachatryan *et al.* (CMS Collaboration), Phys. Rev. D **93**, 072004 (2016).
[22] J. Erdmann, S. Guindon, K. Kroeninger, B. Lemmer, O. Nackenhorst, A. Quadt, and P. Stolte, Nucl. Instrum. Methods Phys. Res., Sect. A **748**, 18 (2014).